Polymer Bulletin (2023) 80:1531–1544
https://doi.org/10.1007/s00289-022-04121-5

ORIGINAL PAPER

Tracing characteristic variations of cellulose nanocrystals during the post-synthesis purification process

Hyeon Jin Yeo[1] · Olajide Emmanuel Adedeji[1,2] · Mi Dan Kang[1] · Hee-Soo Park[1] · Minhye Shin[3] · Dong Hyun Kim[4] · Young Hoon Jung[1]

Received: 4 December 2021 / Revised: 14 January 2022 / Accepted: 29 January 2022 /
Published online: 18 February 2022

Abstract

The production of cellulose nanocrystals (CNC) from biomass involves pretreatment, CNC synthesis, and post-synthesis purification. Information on quality variation during the different stages of pretreatment and CNC synthesis is well documented; however, the post-synthesis purification stage has received little attention. In this study, characteristic variations of CNC during the post-synthesis purification process were investigated. The stages in the process were washing (first and second), neutralization, and centrifugation. CNC's yield decreased after the second washing and neutralization. Cellobiose and cellotriose were detected in the supernatants after the first and second washings. After neutralization, CNC showed a higher colloidal dispersion compared to the first and the second washings. The dimension, morphological, and structural properties were moderately altered during the purification process. Crystallinity increased while crystallite size reduced as CNC purification progressed. The *Ct*CBD3 bound to CNC's surface reduced by 24.27% after the second washing and increased by 47.44% after neutralization. The results in this study provide comprehensive information regarding the overall changes in CNC's characteristics during its purification.

Keywords Cellulose nanocrystals · Crystallinity · Cellulose-binding protein · Surface morphology

Hyeon Jin Yeo and Olajide Emmanuel Adedeji have contributed equally.

✉ Young Hoon Jung
younghoonjung@knu.ac.kr

Extended author information available on the last page of the article

Introduction

Cellulose is an abundant biopolymer and the main constituent of many vegetable biomasses [1]. Cellulose and its derivatives, including cellulose nanocrystals (CNC), carboxymethyl cellulose, methylcellulose, and cellulose nanofibers, have attracted global attention in the past decades due to their surface characteristics, which confer them with a high degree of compatibility and adaptability in many industrial manufacturing processes [2]. In addition to these properties, the CNC has a high level of crystallinity, which has made it an important candidate in biomaterial reinforcement [3, 4].

Cellulose nanocrystal is a crystalline material obtained following acid hydrolysis of cellulose [5]. Conventionally, the production of CNC can be grouped in three stages: biomass pretreatment, CNC synthesis, and post-synthesis purification [6]. The first stage involves the treatment of raw materials with mainly chemicals such as acid and alkali to remove lignin and hemicellulose [2]. In the second stage, the pretreated cellulose-rich biomass is subjected to acid hydrolysis to remove the amorphous region and liberate the crystalline component, CNC [5]. Sulfuric, hydrochloric, nitric, and phosphoric acids are usually employed for the hydrolytic reaction [7]. Among these, sulfuric acid is mostly used due to several advantages, including high reproducibility, uniformity, and ease in process scale-up [6]. During acid hydrolysis of cellulose with sulfuric acid, there is a release of hydroxonium ion, which selectively penetrates and degrades the amorphous region of cellulose [7]. At last, the post-synthesis stage involves the purification of CNC using operations such as washing, neutralization, and centrifugation [8, 9].

The quality of CNC depends on biomass source and the production procedure [10]. Therefore, special attention is given to the selection of appropriate biomasses and subsequent optimization of acid hydrolysis conditions, such as temperature, time, and acid concentration, for improved yield and to achieve the desired surface properties [11–14]. Besides, several studies have reported the modification of biomass pretreatment process to enhance CNC synthesis and, ultimately, improve the overall properties [15–17]. Earlier studies have reported variation in the properties of CNC at different phases of pretreatment and synthesis stages [6, 15]. However, the post-synthesis purification stage has received little attention, hence the focus of this study. In this study, it was hypothesized that the severity of post-synthesis purification would influence the yield and properties of CNC.

Common analytical techniques employed for the characterization of CNC following its production include microscopy, spectrometry, and X-ray diffraction [6, 8, 15]. The use of carbohydrate-binding module (CBM) for the determination of cellulose crystallinity is becoming popular [18–20]. CBM is attaching to specific ligands of insoluble carbohydrates and increasing the specificity and substrate-binding ability of enzymes [21]. This is achieved through stacking or hydrophobic interaction between carbohydrate's sugar rings, CBM's aromatic residues, and the glycan chains [19]. C*t*CBD3 is a CBM from *Clostridium thermocellum,* which

has excellent cellulose-binding properties [22, 23]. Its cellulose-binding property is achieved through the formation of a planar architecture that enhances its complementation with the substrates [24]. Using C*t*CBD3 to determine cellulose, lignin, xylan, and chitin's crystallinity has been reported [22, 23]. Besides, determining CNC's crystallinity using C*t*CBD3 was reported recently [9]. The objective of this study was to evaluate the variation in the properties of CNC during post-synthesis purification stages (washing, neutralization, and centrifugation). The morphology, dimension, structural properties, crystallinity, and protein-binding capacity of CNC were monitored during the stages.

Materials and methods

Materials

Avicel PH-101 was obtained from Sigma-Aldrich (St. Louis, MO, USA), C*t*CBD3 (UniProtKB, Q06851, from *Clostridium thermocellum* ATCC 27405, UniProt Consortium) was procured from the European Bioinformatics Institute, Hinxton Cambridge CB10 1SD, United Kingdom. The characteristic features of *Ct*CBD3 and the cloning of its gene on a pET-21a vector (recombinant *E. coli* BL21 DE3) have been previously described [24]. Sodium hydroxide (Junsei Chemicals, Tokyo, Japan), sulfuric acid (Duksan Pharmaceutical Industry, Gyeonggi-do, Korea), glucose (Sigma-Aldrich), cellobiose (Sigma-Aldrich), cellotriose (Sigma-Aldrich), and uranyl acetate (TED PELLA, Redding, CA, USA) were obtained from Duksan, Ansan, Korea. Luria-Bertani broth (BD, Franklin Lakes, NJ, USA), isopropyl-β-D-thiogalactoside (Sigma-Aldrich), Tris-HCl (Duksan), ampicillin (Sigma-Aldrich), imidazole (Sigma-Aldrich), and Bicinchonic acid assay (BCA) reagent kit (BCA Protein Assay Kit, Thermo Scientific, Waltham, MA, USA) were supplied by Taeyoung, Yeongdeungpo-gu, Seoul, Korea.

Preparation of cellulose nanocrystals

The sulfuric acid hydrolytic method described by So et al. [9] was used for the synthesis of CNC from Avicel. In this study, the synthesis of CNC was considered in four stages: hydrolysis, washing, neutralization, and centrifugation (Fig. 1). Briefly, Avicel (10 g) was hydrolyzed with 175 mL 60 wt% sulfuric acid at 45 °C for 45 min. After acid hydrolysis, 3 L of distilled water was added and the resulting suspension was kept at room temperature (20 ± 2 °C) for 12 h. Subsequently, about 2 L of the supernatant was carefully decanted and the remaining suspension (A1) was collected. The step was repeated, and another suspension (A2) was obtained. Thereafter, sample A2 (1 L) was neutralized with 10 M NaOH and centrifuged at 7,000×*g* for 15 min. The residue obtained was washed several times with distilled water until the water became turbid. The turbid supernatant (TCNC) and pellet particles (PCNC) were collected separately. The yield of the collected CNC samples was

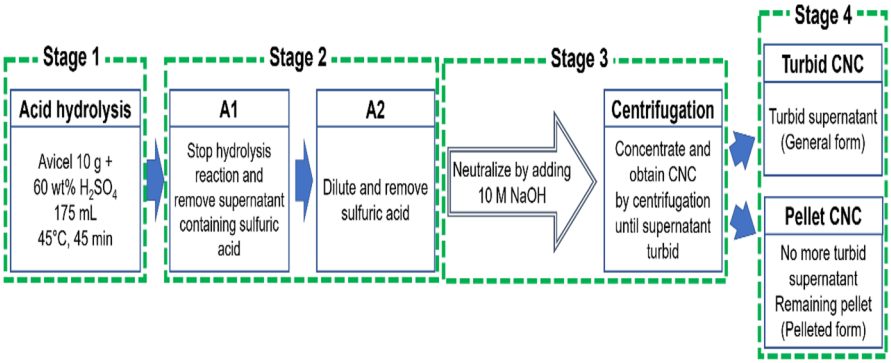

Fig. 1 Purification process of CNC

expressed in percentage. The CNC samples were further characterized to obtain the particle size, dispersibility, morphology, crystallinity, and protein-binding efficiency.

Recovery of *Ct*CBD3

The procedure described by Kim et al. [22] was used for the recovery of *Ct*CBD3 from recombinant *E.* coli. Briefly, recombinant *E. coli* BL21 (DE3) containing the *Ct*CBD3 gene was inoculated into Luria-Bertani broth containing 50 µg/mL of ampicillin and incubated at 37 °C. The absorbance of the medium was monitored at 600 nm during incubation. When the absorbance reached 0.4–0.6, 1 mM isopropyl-β -D-thiogalactoside was added and incubation continued at 37 °C for 4 h. The cells were recovered by centrifugation and resuspended in 50 mM Tris-HCl buffer (pH 8.0). The suspension was sonicated and centrifuged (10,000×*g*, 4 °C, 30 min). The supernatant was purified using Ni-NTA agarose (Qiagen, Hilden, Germany) column pre-stabilized with 50 mM Tris-HCl buffer (pH 8.0). Thereafter, 50 mM Tris-HCl buffer containing 50 mM imidazole was introduced into the column for washing. Subsequently, 50 mM Tris-HCl with 0.1–1.0 M imidazole was added for protein elution.

Analysis of cellulose degradation during cellulose nanocrystal purification

The composition of soluble fractions recovered during the purification of CNC was evaluated using thin layer chromatographic (TLC) analysis [25]. The soluble fractions were introduced into a 20×20 cm silica gel 60 G 25 Glass plates (Merck, Darmstadt, Germany) in a mobile phase consisting of *n*-butanol/acetic acid/water (2:1:1, by volume). This was followed by heating for 15 min at 120 °C. Sulfuric acid solution dissolved in ethanol (10%, v/v) was sprayed onto the plate. Glucose, cellobiose, and cellotriose were used as standards.

The pH of each sample was measured using a pH meter (ORION STAR A215, Thermo Scientific, Waltham, MA, USA).

Determination of dispersibility of cellulose nanocrystals

The sedimentation procedure described by Cheng et al. [8] was used to determine CNC's dispersibility. Suspensions, 0.1–0.5%, of each sample were prepared in transparent bottles and allowed to gravitationally settle for 48 h.

Determination of morphology and dimension of cellulose nanocrystals

Bio-transmission electron microscope, TEM, (Bio-TEM, HT 7700, Hitachi, Tokyo, Japan) was used to measure the shape and size of CNC based on the procedure described by Brinkmann et al. [7]. Samples were dried on a carbon-coated grid and stained with uranyl acetate. The size was measured using the ImageJ software (National Institutes of Health, Rockville Pike, MD, USA) through random sampling of more than 20 individual particles.

X-ray diffractometry and Fourier transform infrared spectroscopy

X-ray diffractometric (XRD, EMPYREAN, Malvern Panalytical, Malvern, UK) analysis was conducted to determine the crystallinity and crystallite size of the samples based on the procedure described by Gong et al. [26]. The samples were freeze-dried before analysis. The freeze-dried sample was ground to an average particle size of 10 µm in a corundum mortar and pestle. The ground sample was poured into the sample holder and XRD patterns were obtained at 40 kV and 100 mA Cu radiation. Diffracted radiations were measured in the range of $2\theta = 5–50°$. The data generated were analyzed using Origin 2021b software (Origin Laboratory Corporation, Northampton, MA 01060, USA). The crystallinity index was estimated as the ratio of the area of the crystalline region and the total area of crystalline and amorphous regions. The crystallite size, D (nm), is calculated using the Scherrer Equation (Eq. 1) [27].

$$D = \frac{K\lambda}{\beta \mathrm{Cos}\theta} \tag{1}$$

where K, λ, β, and θ are Bragg's constant, wavelength of diffracted X-ray, full width at half maximum, and diffraction angle, respectively.

Fourier transform infrared spectroscope (FTIR, Nicolet iS5 FTIR Spectrometer, Thermo Scientific, Waltham, MA, USA) was used to evaluate the structural properties of freeze-dried CNC samples based on the protocol described by Xiao et al. [14]. The analysis was done at a spectra-range of 4000–500 cm^{-1}, 16 scans, and 4 cm^{-1} resolution.

Determination of *Ct*CBD3 binding on cellulose nanocrystals

*Ct*CBD3 binding on CNC was determined based on the procedure described by So et al. [9]. One milligram of CNC was added to a solution containing 200 µg protein in 0.5 mL 50 mM KPO_4 at pH 7.0. The mixture was maintained at 4 °C for 30 min

and, thereafter, centrifuged for 7 min at 13,000×*g* and 4 °C. The amount of residual protein in the supernatant was determined using the BCA assay. The residual protein was deducted from the initial protein weight to obtain the weight of bound protein.

Statistical analysis

All experiments were conducted in triplicates. Data were subjected to analysis of variance and Duncan multiple range test to determine the significant difference ($p < 0.05$) using Statistical Package for the Social Scientist (version 23, IBM Statistics, Armonk, NY, USA).

Results and discussion

Yield of cellulose nanocrystals

The yield of CNC at different stages of purification varied (Table 1). A1 had a yield of 83.36% and this significantly ($p < 0.05$) reduced by 27.77% after the second washing. This high rate of reduction was due to CNC degradation owing to the presence of negatively charged sulfate ester group of sulfuric acid on the surface of CNC [8]. This might affect the dispersibility of CNC and reduce its reinforcing efficiency [7]. There was a further significant ($p < 0.05$) 16.41% reduction after neutralization with NaOH. This showed that NaOH treatment had higher efficiency in reducing the potency of sulfuric acid relative to the use of water. The neutralization with NaOH possibly reduced the concentration of the sulfate ester group, which resulted in a reduction in CNC degradation [8]. These findings showed that the yield of CNC is influenced by the severity of post-hydrolysis treatments. Wang et al. [17] also showed variation in the yield of CNC at different stages of hydrolysis of bleached softwood kraft pulp.

The TLC bands of collected supernatant during CNC purification are shown in Fig. 2. Cellobiose and cellotriose were present in the supernatant after the

Table 1 Yield, dimension, and crystallinity of cellulose nanocrystals at different stages of purification

Parameter	A1	A2	TCNC	PCNC	Avicel
Yield (%)	83.36 ± 3.56^{a}	60.21 ± 4.22^{b}	33.45 ± 1.56^{c}	16.91 ± 0.82^{d}	N.A
pH	0.33 ± 0.02^{c}	0.67 ± 0.02^{b}	6.22 ± 0.24^{a}	N.A	N.A
Length (nm)	165.65 ± 49.77^{a}	130.10 ± 42.27^{a}	153.12 ± 49.81^{a}	N.A	N.A
Width (nm)	14.15 ± 4.88^{a}	11.54 ± 4.34^{a}	12.99 ± 2.23^{a}	N.A	N.A
Aspect ratio	12.39 ± 4.26^{a}	11.57 ± 2.64^{a}	12.11 ± 4.32^{a}	N.A	N.A
Crystallinity (%)	70.08 ± 0.12^{b}	71.96 ± 1.06^{a}	72.61 ± 0.04^{a}	68.91 ± 0.34^{c}	70.94 ± 1.01^{b}
Crystallite size (nm)	4.94 ± 0.44^{a}	4.57 ± 0.11^{b}	4.08 ± 0.05^{c}	4.76 ± 0.02^{ab}	5.10 ± 0.03^{a}

The data from triplicate experiments are expressed as mean ± standard deviation

N.A—Not applicable

Values with different superscripts in row are significantly different ($p < 0.05$)

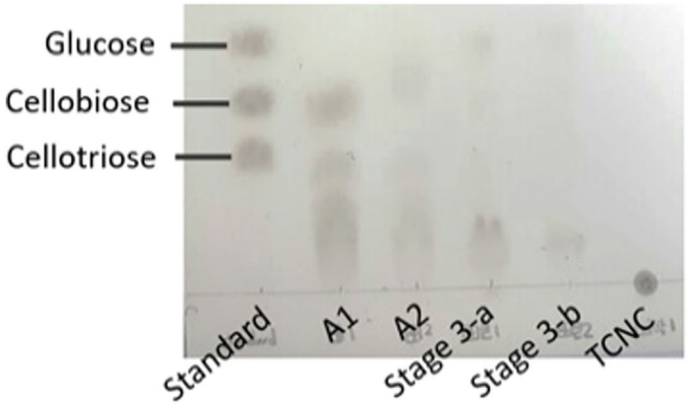

Fig. 2 Thin layer chromatographic results of supernatants at different stages of CNC purification. A1 (lane 2), A2 (lane 3), Stage 3-a (lane 4), Stage 3-b (lane 5), TCNC (lane 6). Lane 1 contains standard glucose, cellobiose, and cellotriose

recovery of A1, owing to the degradation of the amorphous component of Avicel by sulfuric acid. Sulfuric acid has been shown to selectively degrade amorphous cellulose for the liberation of crystallites [6]. Wang et al. [17] also reported the presence of glucose and fructose in the hydrolysate after acid hydrolysis of softwood kraft pulp. The supernatant collected after A2 recovery also showed the presence of cellobiose, and this validated the fact that the presence of adhering sulfate ester group on CNC's surface might cause its degradation. Water and hydroxonium molecules disrupt the hydrogen bonds on cellulose surface, and this culminates in the formation of new hydrogen bonds with the hydroxyl group of the β-1,4 glycosidic bond of cellulose and the protonation of the oxygen atoms of the glycosidic bonds. In the presence of water, there is a breakdown of C–O bonds and conjugate acid to form cyclic carbonium leading to the release of sugars [17]. None of the bands of the standard sugars was detected in the supernatant after neutralization probably due to the inhibition of the sulfate ester group by neutralization reaction [27]. Besides, no sugar was detected in the TCNC. Overall, the result suggested an increasing purity of CNC along the purification path.

The pH of the recovered CNC samples varied (Table 1). An acidic pH was recorded for A1 and A2. The pH of A2 was slightly higher. The adhering sulfate ester group on the CNC surface might be responsible for the low pH. Low CNC surface pH may trigger intra- and inter-molecular hydrogen bonding, which affect crystallinity [14]. The pH of CNC suspension obtained after treatment with NaOH significantly ($p < 0.05$) increased to 6.22 due to the neutralization of sulfuric acid. This is related to the disruption of hydrogen bonds in the crystal region by the hydrated sodium ion [28]. The significantly ($p < 0.05$) higher pH value of TCNC also implies less sulfate ester group on the CNC surface [27].

Dispersion ability of cellulose nanocrystals

The dispersibility of prepared CNC suspensions is shown in Fig. 3. There was variation in the dispersibility of Avicel and the prepared CNC suspensions after 48 h of sedimentation. Avicel did not show any dispersibility because of its large particle size and strong hydrogen bond, which increased surface tension and, by implication, sedimentation [8]. All the CNC suspensions showed good dispersibility, irrespective of the concentration. The TCNC showed higher colloidal dispersion compared to A1 and A2. This is attributed to its low surface area, which increased its homogeneity and reactivity due to strong electrostatic force [8]. The lower dispersibility of A1 and A2 might be due to an increase in the formation of inter-molecular hydrogen bonding by the presence of water molecules [14]. The high dispersibility of TCNC is an indication of good quality, especially in terms of crystallinity, biocompatibility, heat, and colloidal stability [6].

Morphological changes of cellulose nanocrystals during purification

The morphology of CNC at different stages of purification is presented in Fig. 4. The morphology of A1, A2, and TCNC showed a distinctive needle-like structure, which characterizes cellulose I spectrum CNC [7]. The arrangement of the particles in each of the CNC samples differed possibly due to variation in self-orientation and inter-particle distance [29]. This could influence their properties, especially crystallinity [15]. The morphology of PCNC showed an unusual clumping together of particles due to the presence of other compounds. Consequently, its particle size was not measured in this study. The dimension of the CNC samples in this study was within the standard recommendations for diameter (2–20 nm), length (100–600 nm), and aspect ratio (10–100) [30]. The variation was further elucidated in terms of the length, width, and aspect ratio (Table 1). There was no significant difference ($p > 0.05$) among the samples in length, width, and aspect ratio. Nonetheless, A1 had the highest mean values in all the parameters followed by TCNC.

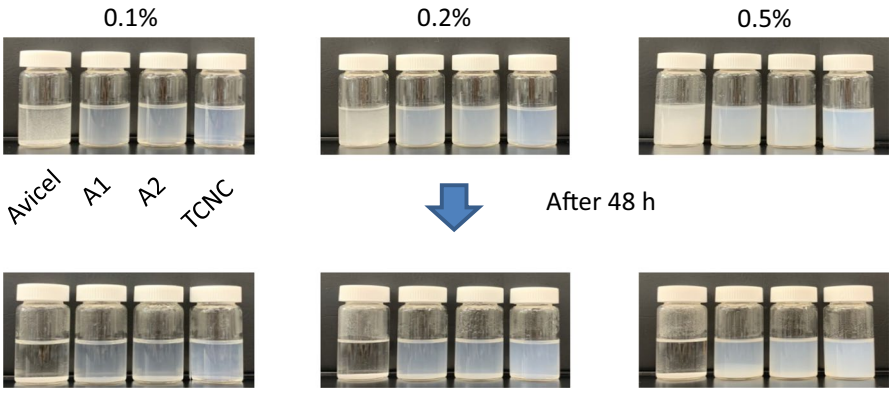

Fig. 3 Dispersibility of Avicel and CNC at different concentrations

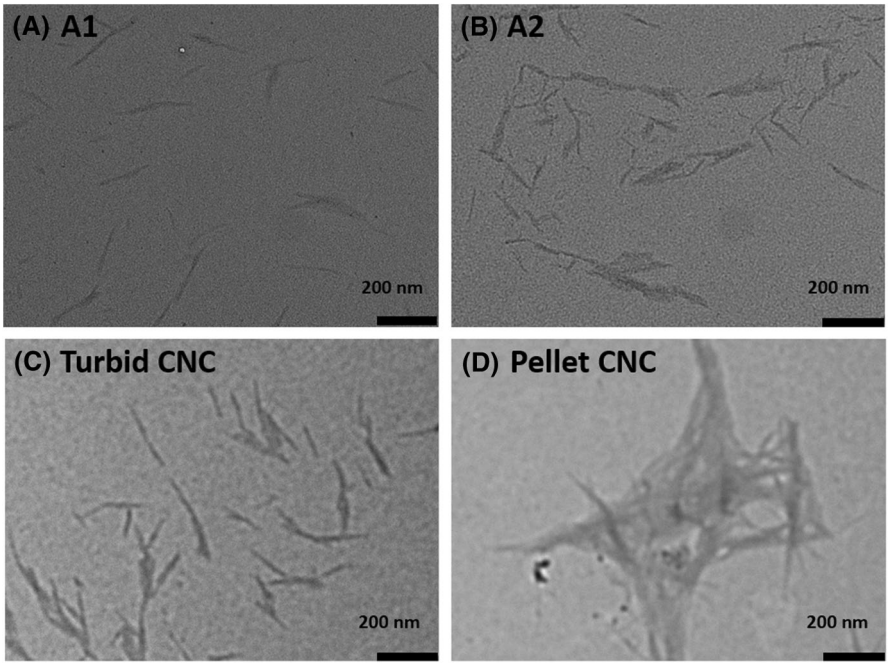

Fig. 4 TEM images of CNC at different stages of purification **A** A1, **B** A2, **C** TCNC, and **D** PCNC

The least ($p > 0.05$) dimension was recorded for A2. This implied that excessive use of water during purification adversely affected the morphology of CNC owing to increased protonation of glycosidic bonds leading to the breakdown of C–O bonds and, consequently, shortening of the particulate sizes [17]. Previous studies [16, 31] also reported variation in the dimension of CNC based on source, pretreatment, and extraction methods.

Crystallinity and structural properties of cellulose nanocrystals

The XRD patterns of Avicel and CNC samples are presented in Fig. 5a. All the samples showed similar absorption peaks, $2\theta = 15.10°$, 16.60°, and 22.50°, that are representative planes for the cellulose I spectrum of CNC [14, 32]. This indicated that the crystalline structure in cellulose I was maintained during hydrolysis and the subsequent purification process. Avicel showed broader and diffused peaks, which are attributed to its higher amorphous region [27], compared to the CNC samples. The sulfuric acid hydrolysis of Avicel might have degraded its amorphous region to yield crystalline cellulose, CNC, which showed distinctive XRD crystalline peaks [7]. Cheng et al. [8] also reported distinct crystalline peaks for CNC following acid hydrolysis of commercial microcrystalline cellulose. The crystallinity and crystallite size of CNC samples varied (Table 1). There was no significant difference ($p > 0.05$) in crystallinity of A1 and Avicel. A significant increase (1.88%) in crystallinity

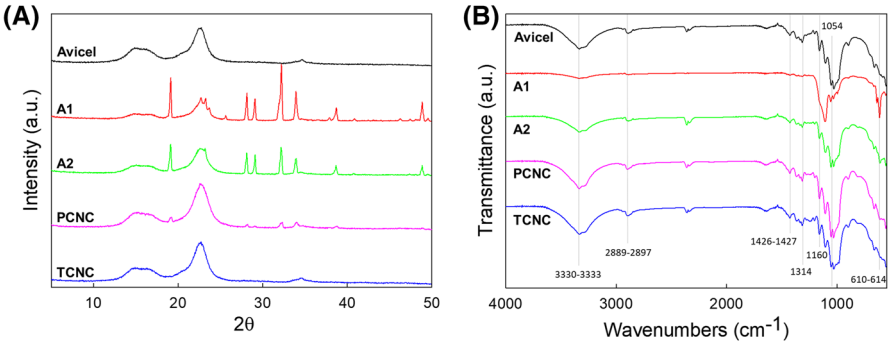

Fig. 5 **A** X-ray diffraction patterns and **B** FTIR spectra of Avicel and CNC at different purification stages

was recorded following the second washing. Neutralization with NaOH gave a further significant increase (0.65%) in crystallinity. This was possibly because of an increased swelling of the crystalline region following the continuous removal of the hydrolyzed amorphous region by water and the neutralization of adhering sulfate ester group on CNC's surface by NaOH [26]. A low crystallite size was reported for Avicel and CNC samples and this implied that the amorphous region was solely responsible for peak broadening [33]. The value in this study was similar to the crystallite size (3.50–4.20 nm) previously reported for CNC synthesized from Avicel [26]. There was a significant ($p < 0.05$) reduction in crystallite size as the purification of CNC progressed due to the variation in the texture of crystallite as well as the crystallinity index of CNC at various purification stages. According to Park et al. [33], the crystallite size of cellulose is dependent on the nature of crystallites, synthesis, and sample preparation methods. TCNC had the least crystallite size because of the rearrangement of CNC's molecular chains following the neutralization of the sulfate ester group of sulfuric acid by NaOH [26].

The structural changes observed during the purification of CNC are shown by the FTIR spectra in Fig. 5b. The absorbance peaks of 3331–3333 cm^{-1} (OH stretching and vibration in cellulose) [34, 35], 2889–2897 cm^{-1} (CH stretching in cellulose), 1636–1653 cm^{-1} (symmetric bending of CH_2) [35], 1314–1315 cm^{-1} (CH_2 rocking) [36], and 1160 cm^{-1} and 1054 cm^{-1} (C–O–C asymmetric stretching and vibration in cellulose) [35] were observed in Avicel and CNC samples. Meanwhile, 610–614 cm^{-1} peaks, indicating C–S stretching [37], appeared in samples A1 and A2 and this is related to the etherification of hydroxyl group owing to the deposition of negatively charged sulfate half esters on the surface of CNC [32].

*Ct*CBD3 binding

The concentration of *Ct*CBD3 bound to the surface of Avicel and CNC samples is presented in Fig. 6. There was significant ($p < 0.05$) variation in the concentration of *Ct*CBD3 bound on these substrates, indicating a variation in the affinity of the CBM to the different substrates [19]. The affinity of a CBM to a substrate is correlated to the substrate's crystallinity, therefore, the low concentration of *Ct*CBD3

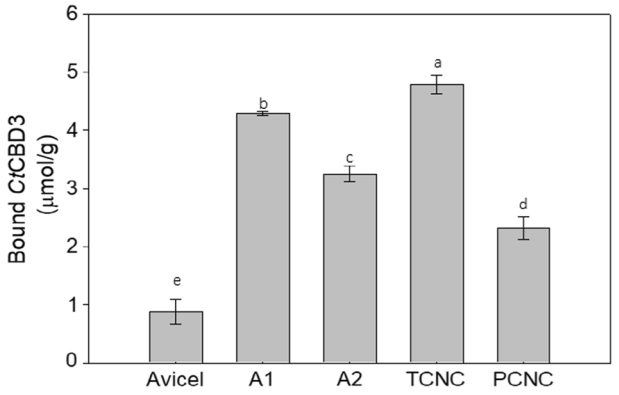

Fig. 6 Binding ability of *Ct*CBD3 on CNC at different purification stages

bound on Avicel is due to the presence of a high amorphous region [23]. Following acid hydrolysis of Avicel, a significant ($p < 0.05$) increase, up to 5.89 fold, in *Ct*CBD3's binding ability was recorded, relating to the increase in crystallinity following the hydrolytic cleavage of glycosidic bonds of the amorphous domain of Avicel by the hydroxonium ions released by the sulfate ester group of sulfuric acid [15]. This corroborated the findings of So et al. [9] who reported a 2.79-fold increase in C*t*CBD3 binding following the synthesis of CNC from Avicel. There was significant ($p < 0.05$) variation in the binding ability of *Ct*CBD3 on CNC based on the stage of recovery during purification. This implied that purification treatments of CNC influenced the adsorption of *Ct*CBD3 on the substrate. This aligned with Liu et al. [19] who reported variation in frequency and dissipation values at the adsorption equilibrium following the use of different concentrations of CBM4 on CNC. The amount of *Ct*CBD3 bound on CNC's surface reduced significantly ($p < 0.05$) by 24.27% after the second washing. This further suggested the detrimental effect of water on the crystallinity of CNC as earlier discussed. The treatment of A2 with NaOH resulted in a 47.44% increase ($p < 0.05$) in the binding ability of *Ct*CBD3 on CNC. This might be linked with the neutralization of adhering sulfuric acid on CNC's surface, thus preventing the disruption of glycosidic bonds on the surface of CNC [17]. Among the CNC samples, *Ct*CBD3 showed the least binding on PCNC due to the presence of other compounds. The result of cellulose-binding experiment agreed with the crystallinity result obtained from XRD.

Conclusions

This study showed variation in the properties of CNC during post-synthesis purification. The yield, morphology, and crystallinity of CNC varied depending on the stage of purification. The crystallinity of CNC increased as purification progressed. The affinity of *Ct*CBD3 on CNC's surface was negatively affected by excessive water treatment. The crystallinity of CNC and its protein-binding capacity increased

following neutralization with NaOH. This study has established the need to optimize CNC purification conditions for improved yield and surface properties.

Acknowledgments This work was supported by the National Research Foundation of Korea (NRF) grant funded by Korean government (Ministry of Science and ICT, MSIT; No 2020R1C1C1005251).

Author contributions HJY performed most experiments, conducted statistical analysis and contributed in writing the draft manuscript. OEA performed statistical analysis, interpreted data and wrote the draft manuscript. MDK, HSO, and HSP performed part of the experiments. MS conducted statistical analysis and performed part of the experiment. DHK reviewed and revised the draft manuscript. YHJ conceived the idea, acquired fund, supervised the project, reviewed, and revised the manuscript. All authors read and approved the final manuscript.

Data and materials availability All data generated or analyzed during this study are included in this article.

Declarations

Conflict of interest The authors declare that they have no known competing financial interest or personal relationship that could have influenced the findings reported in this paper.

References

1. Shaghaleh H, Xu X, Wang S (2018) Current progress in production of biopolymeric materials based on cellulose, cellulose nanofibers, and cellulose derivatives. RSC Adv 8:825–842
2. Thomas B, Raj MC, Athira KB, Rubiyah MH, Joy J, Moores A, Drisko GL, Sanchez C (2018) Nanocellulose, a versatile green platform: from biosources to materials and their applications. Chem Rev 118:11575–11625
3. Catori DM, Fragal EH, Messias I, Garcia FP, Nakamura CV, Rubira AF (2021) Development of composite hydrogel based on hydroxyapatite mineralization over pectin reinforced with cellulose nanocrystal. Int J Biol Macromol 167:726–735
4. Chinta ML, Velidandi A, Pabbathi NPP, Dahariya S, Parcha SR (2021) Assessment of properties, applications and limitations of scaffolds based on cellulose and its derivatives for cartilage tissue engineering: a review. Int J Biol Macromol 175:495–515
5. Huang S, Tao R, Ismail A, Wang Y (2020) Cellulose nanocrystals derived from textile waste through acid hydrolysis and oxidation as reinforcing agent of soy protein film. Polymers 12:958
6. Vanderfleet OM, Cranston ED (2020) Production routes to tailor the performance of cellulose nanocrystals. Nat Rev Mater 6:124–144
7. Brinkmann A, Chen M, Couillard M, Jakubek ZJ, Leng T, Johnston LJ (2016) Correlating cellulose nanocrystal particle size and surface area. Langmuir 32:6105–6114
8. Cheng M, Qin Z, Hu J, Liu Q, Wei T, Li W, Ling Y, Liu B (2020) Facile and rapid one–step extraction of carboxylated cellulose nanocrystals by H2SO4/HNO3 mixed acid hydrolysis. Carbohydr Polym 231:115701
9. So BR, Yeo HJ, Lee JJ, Jung YH, Jung SK (2021) Cellulose nanocrystal preparation from *Gelidium amansii* and analysis of its anti-inflammatory effect on the skin *in vitro* and *in vivo*. Carbohydr Polym 254:117315
10. Gupta GK, Shukla P (2020) Lignocellulosic biomass for the synthesis of nanocellulose and its ecofriendly advanced applications. Front Chem 8:601256
11. Benito-Gonzalez I, Lopez-Rubio A, Gavara R, Martınez-Sanz M (2019) Cellulose nanocrystal-based films produced by more sustainable extraction protocols from *Posidonia oceanica* waste biomass. Cellulose 26:8007–8024
12. Grishkewich N, Mohammed N, Tang J, Tam KC (2017) Recent advances in the application of cellulose nanocrystals. Curr Opin Colloid Interface Sci 29:32–45

13. Tang J, Sisler J, Grishkewich N, Tam KC (2017) Functionalization of cellulose nanocrystals for advanced applications. J Colloid Interface Sci 494:397–409
14. Xiao Y, Kang S, Liu Y, Guo X, Li M, Xu H (2021) Effect and mechanism of calcium ions on the gelation properties of cellulose nanocrystals-whey protein isolate composite gels. Food Hydrocoll 111:106401
15. Hernandez CC, Ferreira FF, Rosa DS (2018) X-ray powder diffraction and other analyses of cellulose nanocrystals obtained from corn straw by chemical treatments. Carbohydr Polym 193:39–44
16. Luzi F, Puglia D, Sarasini F, Tirillò J, Maffei G, Zuorro A, Lavecchia R, Kenny JM, Torre L (2019) Valorization and extraction of cellulose nanocrystals from North African grass: *Ampelodesmos mauritanicus* (Diss). Carbohydr Polym 209:328–337
17. Wang J, Xu J, Zhu S, Wu Q, Li J, Gao Y, Wang B, Li J, Gao W, Zeng J, Chen K (2021) Preparation of nanocellulose in high yield via chemi-mechanical synergy. Carbohydr Polym 251:117094
18. Duan CJ, Huang MY, Pang H, Zhao J, Wu CX, Feng JX (2017) Characterization of a novel theme C glycoside hydrolase family 9 cellulase and its CBM-chimeric enzymes. Appl Microbiol Biotechnol 101:5723–5737
19. Liu T, Zhang Y, Lu X, Wang P, Zhang X, Tian J, Wang Q, Song J, Jin Y, Xiao H (2021) Binding affinity of family 4 carbohydrate binding module on cellulose films of nanocrystals and nanofibrils. Carbohydr Polym 251:116725
20. Oliveira C, Romani A, Gomes D, Cunha JT, Gama FM, Domingues L (2018) Recombinant family 3 carbohydrate-binding module as a new additive for enhanced enzymatic saccharification of whole slurry from autohydrolyzed *Eucalyptus globulus* wood. Cellulose 25:2505–2514
21. Maharjan A, Alkotaini B, Kim BS (2018) Fusion of carbohydrate binding modules to bifunctional cellulase to enhance binding affinity and cellulolytic activity. Biotechnol Bioprocess Eng 23:79–85
22. Kim IJ, Ko HJ, Kim TW, Nam KH, Choi IG, Kim KH (2013) Binding characteristics of a bacterial expansin (BsEXLX1) for various types of pretreated lignocellulose. Appl Microbiol Biotechnol 97:5381–5388
23. Kim IJ, Ko H, Kim T, Choi CI, Kim KH (2013) Characteristics of the binding of a bacterial expansin (BsEXLX1) to microcrystalline cellulose. Biotechnol Bioeng 110:401–407
24. Hashimoto H (2006) Recent structural studies of carbohydrate-binding modules. Cell Mol Life Sci 63:2954–2967
25. Nishida Y, Suzuki K, Kumagai Y, Tanaka H, Inoue A, Ojima T (2007) Isolation and primary structure of a cellulase from the Japanese sea urchin strongylocentrotus nudus. Biochimie 89:1002–1011
26. Gong J, Li J, Xu J, Xiang Z, Mo L (2017) Research on cellulose nanocrystals produced from cellulose sources with various polymorphs. RSC Adv 7:33486–33493
27. Pandi N, Sonawane SH, Kishore KA (2021) Synthesis of cellulose nanocrystals (CNCs) from cotton using ultrasound-assisted acid hydrolysis. Ultrason Sonochem 70:105353
28. Wu Q, Xu J, Zhu S, Kuanga Y, Wang B, Gao W (2020) Crystalline stability of cellulose III nanocrystals in the hydrothermal treatment and NaOH solution. Carbohydr Polym 249:11682
29. Jiang H, Wu Y, Han B, Zhang Y (2017) Effect of oxidation time on the properties of cellulose nanocrystals from hybrid poplar residues using the ammonium persulfate. Carbohydr Polym 174:291–298
30. Jung YH (2017) Trends and prospects of microfibrillated cellulose in bio-industries. Microbiol Biotechnol Lett 45:1–11
31. Melikoğlu AY, Bilek SE, Cesur S (2019) Optimum alkaline treatment parameters for the extraction of cellulose and production of cellulose nanocrystals from apple pomace. Carbohydr Polym 215:330–337
32. Qiao C, Chen G, Zhang J, Yao J (2016) Structure and rheological properties of cellulose nanocrystals suspension. Food Hydrocoll 55:19–25
33. Park S, Baker JO, Himmel ME, Parilla PA, Johnson DK (2010) Cellulose crystallinity index: measurement techniques and their impact on interpreting cellulase performance. Biotechnol Biofuels 3:10
34. El-Achaby M, Kassab Z, Aboulkas A, Gaillard C, Barakat A (2018) Reuse of red algae waste for the production of cellulose nanocrystals and its application in polymer nanocomposites. Int J Biol Macromol 106:681–691
35. Aguayo MG, Perez AF, Reyes G, Oviedo C, Gacitúa W, Gonzalez R, Uyarte O (2018) Isolation and characterization of cellulose nanocrystals from rejected fibers originated in the kraft pulping process. Polymers 10:1145

36. Chieng BW, Lee SH, Ibrahim NA, Then YY, Loo YY (2017) Isolation and characterization of cellulose nanocrystals from oil palm mesocarp fiber. Polymers 9:355
37. Lamaming J, Hashim R, Leh CP, Sulaiman O, Sugimoto T, Nasir M (2015) Isolation and characterization of cellulose nanocrystals from parenchyma and vascular bundle of oil palm trunk (*Elaeis guineensis*). Carbohydr Polym 134:534–540

Authors and Affiliations

Hyeon Jin Yeo[1] · Olajide Emmanuel Adedeji[1,2] · Mi Dan Kang[1] · Hee-Soo Park[1] · Minhye Shin[3] · Dong Hyun Kim[4] · Young Hoon Jung[1]

[1] School of Food Science and Biotechnology, Kyungpook National University, Daegu 41566, Republic of Korea

[2] Department of Food Science and Technology, Federal University Wukari, P.M.B. 1020, Wukari, Nigeria

[3] Department of Microbiology, Inha University School of Medicine, Incheon 22212, Republic of Korea

[4] Department of Marine Food Science and Technology, Gangneung-Wonju National University, Gangneung, Gangwon 25457, Republic of Korea